Journal of Pharmaceutical and Biomedical Analysis 129 (2016) 172–181

Contents lists available at ScienceDirect

Journal of Pharmaceutical and Biomedical Analysis

journal homepage: www.elsevier.com/locate/jpba

Near infra red spectroscopy as a multivariate process analytical tool for predicting pharmaceutical co-crystal concentration

Clive Wood[a,*], Abdolati Alwati[a], Sheelagh Halsey[b], Tim Gough[a], Elaine Brown[a], Adrian Kelly[a], Anant Paradkar[a]

[a] Centre for Pharmaceutical Engineering Science, University of Bradford, BD7 1DP, UK
[b] Thermo Fisher Scientific, Stafford House, Boundary Way, Hemel Hempstead, HP2 7GE, UK

ARTICLE INFO

Article history:
Received 11 March 2016
Received in revised form 5 June 2016
Accepted 7 June 2016
Available online 7 June 2016

Keywords:
Co-crystal
NIR spectroscopy
Partial least squares
Prediction
Active pharmaceutical ingredient
Process analytical tool

ABSTRACT

The use of near infra red spectroscopy to predict the concentration of two pharmaceutical co-crystals; 1:1 ibuprofen–nicotinamide (IBU-NIC) and 1:1 carbamazepine–nicotinamide (CBZ-NIC) has been evaluated. A partial least squares (PLS) regression model was developed for both co-crystal pairs using sets of standard samples to create calibration and validation data sets with which to build and validate the models. Parameters such as the root mean square error of calibration (RMSEC), root mean square error of prediction (RMSEP) and correlation coefficient were used to assess the accuracy and linearity of the models. Accurate PLS regression models were created for both co-crystal pairs which can be used to predict the co-crystal concentration in a powder mixture of the co-crystal and the active pharmaceutical ingredient (API). The IBU-NIC model had smaller errors than the CBZ-NIC model, possibly due to the complex CBZ-NIC spectra which could reflect the different arrangement of hydrogen bonding associated with the co-crystal compared to the IBU-NIC co-crystal. These results suggest that NIR spectroscopy can be used as a PAT tool during a variety of pharmaceutical co-crystal manufacturing methods and the presented data will facilitate future offline and in-line NIR studies involving pharmaceutical co-crystals.

1. Introduction

Pharmaceutical ingredients have conventionally been manufactured using batch processing with offline laboratory analysis of samples to evaluate the quality and efficacy of the process. However, in-line analytical measurements are now possible during manufacturing, providing significant scope for improving the manufacturing process [1].

In-line monitoring of changes which occur during the manufacturing process can greatly increase process understanding and identification of key parameters [2]. This concept of analysing at the manufacturing stage can be carried out using process analytical technology (PAT) and a quality by design (QbD) methodology. The latest FDA guideline report for process analytical technology states 'Quality cannot be tested into products; it should be built-in or should be by design' [1].

PAT tools form a vital part of the overall PAT framework. Put simply, they are process analysers which are used for monitoring a process. Combined with a QbD approach, the process can be optimised with careful planning, design and using feedback from the PAT tools. Parameters and variables can be adjusted accordingly to suit the manufacturing needs and to achieve a specified outcome or product. PAT tools have now become a necessary technology to use when designing and improving the manufacture of pharmaceutical materials [3]. A large proportion of PAT tools are spectroscopic techniques which often use the infra red, near infra red, X-ray, Raman and ultra violet wavelengths [4]. Currently, numerous spectroscopic techniques combined with multivariate analysis, such as partial least squares (PLS) and principal component analysis (PCA), are being used for evaluation of the pharmaceutical properties of powder, granules, tablets and so forth. An increasingly popular spectroscopic technique is near infra red (NIR) spectroscopy. NIR is extensively used in the pharmaceutical field and is utilised in many areas of production including raw material identification, processing control and final product analysis. It is considered as a process analyser, because of its ability to give multivariate qualitative [5], quantitative [6], physical and chemical [7] information about a material. In addition, NIR spectroscopy can generally penetrate further into solid materials compared to mid-IR, and is therefore

* Corresponding author.
E-mail address: clivewood@outlook.com (C. Wood).

http://dx.doi.org/10.1016/j.jpba.2016.06.010

commonly used to determine the purity of pharmaceutical materials such as excipients prior to the manufacturing processes [8].

Solid state characterisation techniques combined with multivariate analysis and chemometrics have been used for pharmaceutical co-crystal quantification in recent years. Caliandro et al. [9] in 2013, used both XRD and FT-IR combined with multivariate analysis to quantify carbamazepine I, carbamazepine III, saccharin and 1:1 carbamazepine-saccharin co-crystals. Similarly, in 2014 Soares and Carneiro [10] were able to evaluate the synthesis of 1:1 IBU-NIC co-crystals using Raman, powder X-ray diffraction (PXRD) and differential scanning calorimetry (DSC) with partial least squares regression and chemometric pre-treatments. Multivariate calibration is achieved by preparing a set of calibration samples with known analyte concentrations, measuring the spectral response and using the spectral data with a regression method, such as principal component regression (PCR) or PLS, to model the analyte concentration. The outcome is a regression vector which can be optimised and the optimal model is used to predict the analyte concentration (or other properties) in unknown samples [11].

Pharmaceutical co-crystals have the potential to enhance the physicochemical properties of drug compounds [12]. Historically, co-crystals have been referred to as molecular complexes [13,14]. There are now several published definitions to distinguish co-crystals from polymorphs, salts, hydrates, solvates and amorphous materials. In 2005, Aakeröy and Salmon [15] proposed the following definition for a co-crystal; "co-crystals are structurally homogeneous crystalline materials containing two or more components present in stoichiometric amounts, the components are discrete neutral molecular reactants which are solids at ambient temperature". Similarly, a pharmaceutical co-crystal is a co-crystal where one of the components is an active pharmaceutical ingredient (API) with suitable co-former(s) [12].

Reported methods for the preparation of co-crystals include solution crystallisation or solution mediated phase transformation [16], solid-state grinding [17], liquid assisted grinding [18] or solvent-drop grinding [19], hot melt extrusion [20] and ultrasound assisted cocrystallization [21]. For the analysis and characterisation of pharmaceutical co-crystals, popular techniques include PXRD and DSC, usually combined with other techniques such as Raman, NIR, or IR spectroscopy.

Demonstrated by Kelly et al. [22] in 2012, NIR can be used as an in-line PAT tool during the formation of 1:1 IBU-NIC co-crystals using hot melt extrusion (HME). The team were able to identify key band shifts and band formations; particularly in the region 5200–4700 cm^{-1}, when comparing the spectra of processed samples to the 1:1 physical mixture of the starting components. Similarly, Moradiya et al. [23] in 2014 used NIR for in-line characterisation during HME of carbamazepine-cinnamic acid co-crystals allowing determination of the position along the extruder barrel where co-crystal formation commenced by identifying NIR band shifts. A case study, in 2014, using furosemide-adenine co-crystals was used to demonstrate chemometric assisted NIR spectral analysis with PCA which was able to pinpoint cocrystallization nucleation and solvent evaporation events during a solvent evaporation method [24]. This case study then promoted further studies where Sarraguça et al. monitored cocrystallization using NIR spectroscopy for furosemide-nicotinamide and furosemide–*p*-aminobenzioc acid co-crystals during solvent evaporation [25,26]. Carbamazepine-saccharin co-crystals [27] and indomethacin-saccharin co-crystals [28] have also been monitored during antisolvent cocrystallization.

For the present study, two co-crystal pairs were chosen for investigation using NIR spectroscopy; 1:1 ibuprofen-nicotinamide and 1:1 carbamazepine-nicotinamide. Ibuprofen is a nonsteroidal anti-inflammatory drug (NSAID) and is the safest NSAID according to the spontaneous adverse drug reaction reporting system situated in the United Kingdom [29]. It suffers from high permeability and low aqueous solubility and is classified as a class II NSAID according to the biopharmaceutical classification system (BCS) [30]. Carbamazepine is an API normally associated with the treatment of epilepsy and trigeminal neuralgia. It also suffers from poor aqueous solubility and belongs to class II of the BCS [31]. Crucially, both pairs can form a stable co-crystal when paired with suitable co-formers. It has been shown that when ibuprofen and carbamazepine form a co-crystal with the co-former nicotinamide, their aqueous solubilities improve [32].

The aim of this study was to utilise PLS regression to create models which can predict the co-crystal concentration in a powder mixture of the co-crystal and the API using NIR spectroscopy for two co-crystals: 1:1 ibuprofen-nicotinamide and 1:1 carbamazepine-nicotinamide. The spectral information and regression results gathered by this study will assist the development of cocrystallization techniques which do not involve any solvents or additives during the process. Cocrystallization methods, such as ultrasound assisted cocrystallization and hot melt extrusion are increasingly being investigated because of their solvent-free capabilities and ease of scale-up. This study is a step towards realising the potential of these technologies for pharmaceutical cocrystallization purposes by providing a co-crystal quantification platform. In addition, the data from this study will aid future in-line NIR monitoring of pharmaceutical co-crystals. If co-crystal quantification can be achieved throughout the manufacturing stage of pharmaceutical co-crystals, the process can be optimised and co-crystal properties tailored for specific needs.

2. Materials and methods

Ibuprofen, nicotinamide and carbamazepine were all purchased from Sigma Aldrich. The ethanol solvent used for solution evaporation was of analytical grade.

2.1. IBU-NIC co-crystal molecular structure

The hydrogen bonding patterns are well documented for the 1:1 IBU-NIC co-crystal. The racemic ibuprofen binds to nicotinamide via an acid-pyridine motif, before a pair of dimers come together through an amide-amide motif between the nicotinamide molecules. Finally an amide-acid motif forms between the nicotinamide and the ibuprofen to create a 'supramolecular macrocycle structure' [33] (Fig. 1).

2.2. CBZ-NIC co-crystal molecular structure

In this 1:1 co-crystal, a translation related hydrogen-bonding pattern exists between the nicotinamide molecules and the carbamazepine molecules. The donors and acceptors of both amide groups are fulfilled but the nitrogen atom within the ring structure of nicotinamide does not form any strong hydrogen bonds. The crystal packing suggests hydrophobic interlocking rows with $\pi\ldots\pi$ interactions between the carbamazepine and the nicotinamide rings [34] (Fig. 2).

2.3. Preparation of IBU-NIC co-crystals

The methods of preparation for both co-crystal pairs were chosen according to their efficacy and repeatability, several different techniques were trialled before the final methods were selected. Solvent mediated cocrystallization was carried out using a microwave reactor (Monowave 300, Anton Paar GmbH, Austria). 1:1 equimolar weights of ibuprofen and nicotinamide, totalling 0.820 g, were mixed with 82 μL of diluted water in a 30 mL capacity glass tube. The temperature was set to 80 °C and samples were

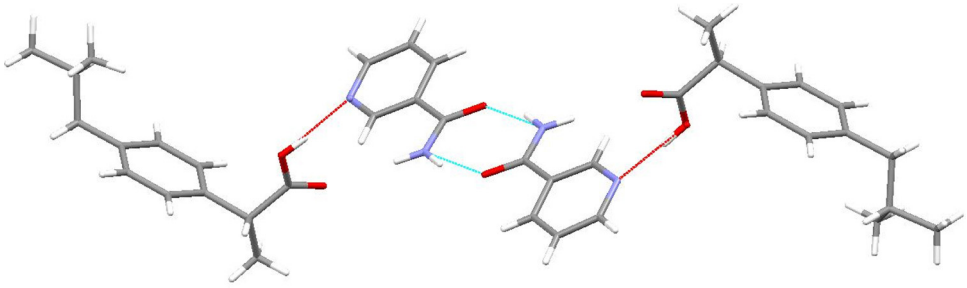

Fig. 1. 1:1 IBU-NIC co-crystal molecular structure. Hydrogen bonding is shown by light blue and red dashed lines. (For interpretation of the references to colour in this figure legend, the reader is referred to the web version of this article.)
Source: Fleischman et al. [34] 2003 via Cambridge Structural Database [35].

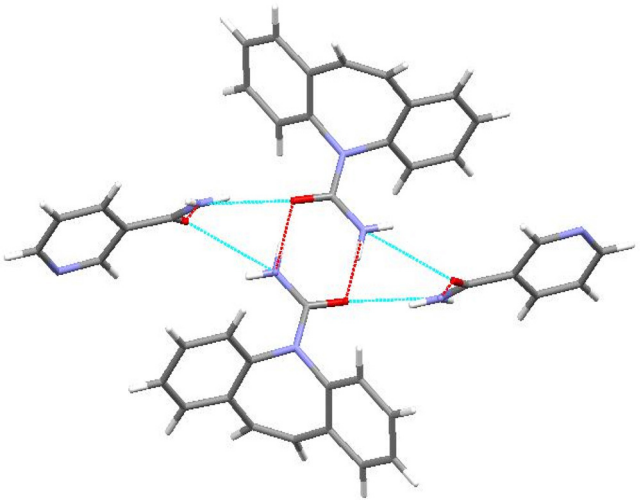

Fig. 2. 1:1 CBZ-NIC co-crystal molecular structure. Hydrogen bonding is shown by light blue and red dashed lines. (For interpretation of the references to colour in this figure legend, the reader is referred to the web version of this article.)
Source: Berry et al. [36] 2008 via Cambridge Structural Database [35].

subjected to microwave irradiation with a holding time of 5 min and were then cooled to 40 °C and held for 1 min.

2.4. Preparation of CBZ-NIC co-crystals

Solvent evaporation was carried out based on the method reported by Shayanfar et al. [37] in 2014. 1:1 equimolar weights of carbamazepine (2.363 g, 0.01 mol) and nicotinamide (1.221 g, 0.01 mol) were dissolved in 20 mL of absolute ethanol. The mixture was gently heated and manually stirred with a glass rod for 30 min. Finally the mixture was left for 72 h at room temperature to evaporate.

2.5. Material analysis

PXRD was carried out using a Bruker D8 X-ray diffractometer. Scans from 2 to 30° (2theta) with a 0.01° step width and a 1s time count were carried out for all samples using CuKα_1 radiation (1.5406 Ang wavelength). The receiving slit was 1° and the scattering slit, 0.2°. DSC was carried out using a Q2000 Differential Scanning Calorimeter (TA Instruments, USA). The general heating profile used was a ramp from 40 to 200 °C with a heating rate of 10 °C/min.

2.6. Collection of NIR spectra

All NIR spectra were collected using an Antaris II NIR spectrometer (Thermo Scientific, UK) in diffuse reflectance mode. Each sample was placed in a standard glass vial which in turn was placed upon the integrating sphere diffuse reflection accessory. Each sample reading averaged 32 individual spectra at a resolution of 8 cm^{-1} and were scanned over the region 4000–10000 cm^{-1} wavenumbers (2500–1000 nm wavelength) using Thermo Scientific RESULT software. For each spectrum, 1557 data points were collected. The software used a standard workflow to minimise interference from the glass vial and collected a background before every individual scan. To increase the signal to noise ratio, each sample was scanned five times and a composite spectrum was created using TQ Analyst software (Thermo Scientific, UK).

2.7. Samples

For the IBU-NIC co-crystal system, a PLS regression model was designed using a set of standard samples consisting of a mixture of 1:1 IBU-NIC co-crystal and pure ibuprofen. The model for the CBZ-NIC system was designed using a set of standard samples consisting of a mixture of 1:1 CBZ-NIC co-crystal and pure carbamazepine. The co-crystals used for the calibration and validation samples were made using the methods described in Sections 2.3 and 2.4. The validation samples were made from a separate batch of co-crystal to the calibration samples for both co-crystals, they were not used to create the PLS models, but they were used to validate the models. The concentration of the calibration samples ranged from pure ibuprofen/carbamazepine (0%) to 100% 1:1 co-crystal with standards made at concentrations of 5% increments in between, totalling 20 calibration samples. Validation samples were made at the following concentrations: 2.5, 7.5, 12.5, 17.5, 27.5, 37.5, 52.5, 62.5, 72.5 and 92.5% 1:1 co-crystal, totalling 10 validation samples.

2.8. PLS regression conditions

The software used for PLS regression and chemometric pretreatments was TQ Analyst (Thermo Scientific, UK). PLS finds the most relevant components based on those that maximise the covariance between the data matrix and the response vector. Combined with linear regression, PLS can predict the response of a validation data set. PLS regression was performed using the averaged IBU-NIC or CBZ-NIC calibration and validation samples. The data was mean centred every time the PLS analysis was performed.

Nine different NIR regions were evaluated for each model. The whole region (10000–4000 cm^{-1} wave numbers) was selected, then relatively large regions to avoid areas affected by noise were chosen. Next, medium sized regions of interest were selected

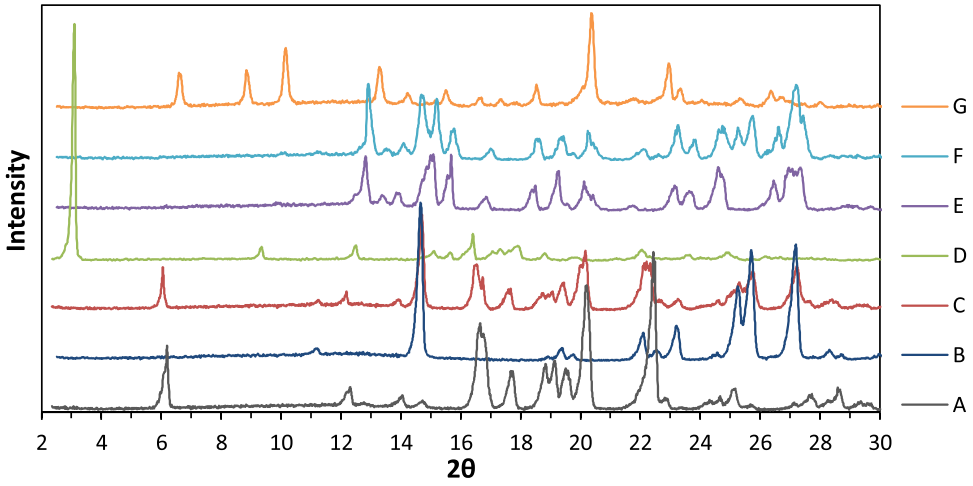

Fig. 3. PXRD diffractograms of (A) IBU, (B) NIC, (C) 1:1 IBU-NIC PM, (D) 1:1 IBU-NIC CC, (E) CBZ, (F) 1:1 CBZ-NIC PM and (G) 1:1 CBZ-NIC CC.

followed by small sized regions which generally covered a small number of bands of interest.

The cross-validation was analysed for each model and the cross validation error did not significantly improve when using more than 2 factors in the majority of cases. Since the models were created using 20 calibration samples, using more than 2 factors could have caused over-fitting of the curves which could result in poor prediction capabilities.

Five types of chemometric pre-treatments were used for both co-crystal pairs which included the standard normal variate (SNV) [38], first and second derivatives, Savitzky-Golay smoothing (SGS) [39] and Norris smoothing (NS) algorithms [40]. SNV pre-treatment was used to compensate for differences in sample pathlength. The SNV was carried out over the full spectral range (10000–4000 cm^{-1} wavenumbers) and effectively minimised any scaling or offset effects which may have occurred.

First and second derivatives were used to improve the resolution of overlapping bands, whilst also acting as a linear baseline correction method. It was beneficial to view individual spectra in the 2nd derivative to locate important bands which increase/decrease in intensity and may shift to different wavenumbers when the co-crystal concentration increased.

Smoothing techniques were applied to reduce noise. SGS was carried out using 7 data points and a polynomial order of 3. NS was carried out using a segment length of 5 and a gap between segments length of 5. Both smoothing techniques can affect the performance of a PLS model.

3. Material characterisation

Pure 1:1 IBU-NIC and 1:1 CBZ-NIC co-crystals were used to create the PLS regression models. PXRD and DSC techniques were used to determine the purity of the synthesised co-crystals. Fig. 3 shows the PXRD spectra for ibuprofen, nicotinamide, 1:1 IBU-NIC physical mixture (PM) and 1:1 IBU-NIC co-crystal (CC). Also displayed are the PXRD spectra for carbamazepine, 1:1 CBZ-NIC PM and 1:1 CBZ-NIC CC.

The PXRD peak at ~3.1° (2θ) is a good indicator of 1:1 IBU-NIC CC and is commonly compared with the ibuprofen peak situated at ~6° (2θ) to determine the purity of the co-crystal. If the co-crystal is pure, then the peak at ~6° (2θ) will not be present in the spectrum. In Fig. 3, it is clear that the ibuprofen peak is absent in the 1:1 IBU-NIC CC. The 1:1 CBZ-NIC CC has characteristic peaks located at approximately 6.7°, 9° and 10.15° (2θ). The carbamazepine peak at 12.8° (2θ) and the nicotinamide peak at 14.65° (2θ) are indicators for any remaining carbamazepine or nicotinamide in the co-crystal sample. It is clear from the 1:1 CBZ-NIC CC spectrum that no residual carbamazepine or nicotinamide were present.

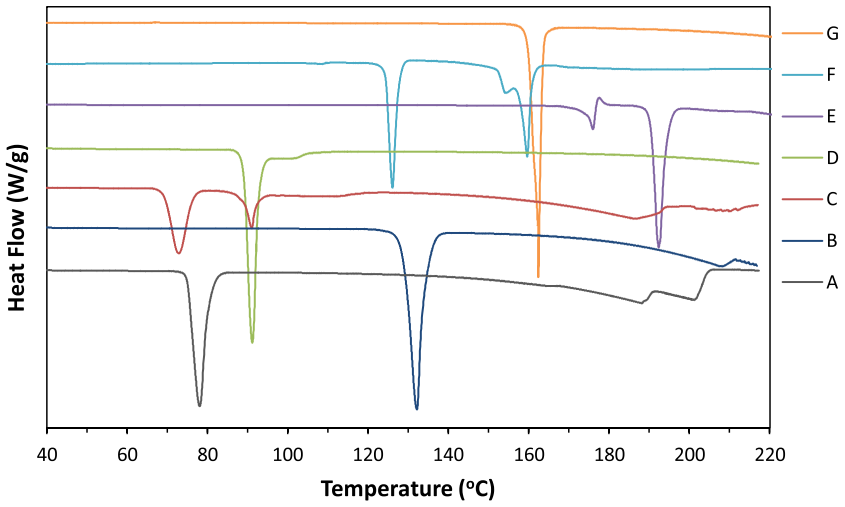

Fig. 4. DSC thermograms for (A) IBU, (B) NIC, (C) 1:1 IBU-NIC PM, (D) 1:1 IBU-NIC CC, (E) CBZ, (F) 1:1 CBZ-NIC PM and (G) 1:1 CBZ-NIC CC.

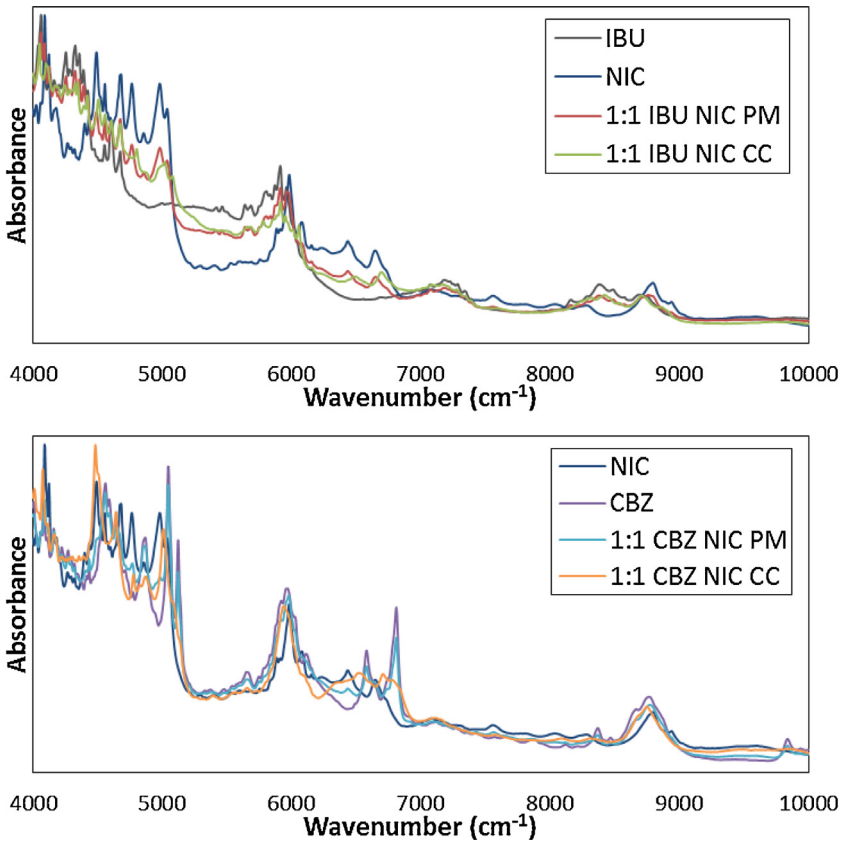

Fig. 5. NIR spectra for IBU, NIC, 1:1 IBU-NIC PM, 1:1 IBU-NIC CC, CBZ, 1:1 CBZ-NIC PM and 1:1 CBZ-NIC CC. For this figure, the spectra were pre-treated using SNV across the whole region 10000–4000 cm^{-1}.

DSC thermograms of ibuprofen, nicotinamide, 1:1 IBU-NIC PM and 1:1 IBU-NIC CC are shown in Fig. 4 along with carbamazepine, 1:1 CBZ-NIC PM and 1:1 CBZ-NIC CC thermograms.

The melting points of ibuprofen and nicotinamide were found to be 78.0 °C and 132.1 °C respectively. The eutectic point of 1:1 IBU-NIC PM was 72.8 °C and the melting endotherm situated at 91.0 °C was attributed to the 1:1 IBU-NIC CC melting point. The pure 1:1 IBU-NIC CC had a melting point of 91.1 °C. The DSC data confirms that cocrystallization of ibuprofen and nicotinamide occurs during the application of a standard temperature ramp.

For pure carbamazepine, there were two endothermic peaks located at 175.9 °C and 192.3 °C which are associated with the melting points of carbamazepine forms III and I respectively. The exothermic peak at 177.5 °C indicates that the crystallisation of carbamazepine form I occurs after form III has melted. The eutectic point of 1:1 CBZ-NIC PM was 126.0 °C and the melting point of 1:1 CBZ-NIC CC was 162.4 °C.

NIR spectra were collected for ibuprofen, nicotinamide, 1:1 IBU-NIC PM, 1:1 IBU-NIC CC, carbamazepine, 1:1 CBZ-NIC PM and 1:1 CBZ-NIC CC. The spectra are shown in Fig. 5.

The physical mixtures for both IBU-NIC and CBZ-NIC pairs display a combination of the characteristic bands from the respective individual components. 1:1 IBU NIC CC had unique bands at approximately 4794, 5087, 6460, 6676, 8285 and 8393 cm^{-1}, 1:1 CBZ-NIC CC also had unique bands at approximately 4636, 5002, 6495 and 6696 cm^{-1}, compared to the respective individual components and their physical mixtures.

4. IBU-NIC PLS model

The RMSEC, RMSEP and correlation coefficient values were recorded for each region and various degrees of chemometric pre-treatments were used. Tables 1 and 2 display the RMSEC and RMSEP values for each regression model respectively. The results suggest that the level of chemometrics used had a significant impact on both error values. The most significant reduction of the RMSEC and RMSEP values was caused by applying the SNV. After using the SNV, the evaluated regions then reacted differently to the various levels of chemometrics. The ten models with the lowest RMSEC values are highlighted in bold to help visualise their distribution related to the different chemometrics that were applied.

Table 3 shows the ten PLS regression models which exhibited the lowest RMSEC values. The correlation coefficient values for the models indicated that they were all well correlated linear models. The difference between the RMSEC and RMSEP values were shown to give an indication of the variance between the calibration and validation data sets.

The wavenumber region of 7450–4700 cm^{-1} provided the smallest calibration error of 0.77% when the 2nd Dev., SNV and NS were applied. This region provided a model with relatively low error values which could accurately predict the percentage yield of 1:1 IBU-NIC CC in samples where there is a mixture of ibuprofen and the 1:1 IBU-NIC CC. This model (Model 1) exhibited a small RMSEP value of 0.95% and the difference between the RMSEC and RMSEP values was only 0.18%. A small difference is a good indicator of the accuracy and predictability of the model.

Model 1 is plotted in Fig. 6. Both the averaged calibration and validation samples are shown to compare the measured co-crystal yield to the PLS regression predicted co-crystal yield. This model had a correlation coefficient of 0.9997 and no outlying points were observed.

The spectral and concentration factor loadings for both PLS factors were calculated. The first factor used 99.1% spectral infor-

Table 1
IBU-NIC model: A matrix of RMSEC values of the PLS regression models when using different regions and different levels of chemometrics (Bold = top ten models).

Region (Wavenumber cm^{-1})	RMSEC Values (%)							
	Original	SNV	1st Dev. SNV	1st Dev. SNV SGS	1st Dev. SNV NS	2nd Dev. SNV	2nd Dev. SNV SGS	2nd Dev. SNV NS
10000–5400	7.17	1.20	1.08	1.08	**0.97**	1.11	1.13	1.10
10000–4000	2.21	1.14	1.67	1.67	1.38	1.83	1.79	1.54
9000–8000	6.07	2.60	**0.87**	**0.90**	1.07	**0.89**	**0.96**	1.11
9000–4700	1.96	1.05	1.03	1.03	**0.92**	1.10	**0.96**	1.06
7450–7000	6.17	3.04	1.01	0.99	1.85	1.22	0.99	**0.77**
6820–6620	4.99	2.98	2.93	2.94	3.10	3.22	2.66	2.94
6100–5600	5.12	1.09	1.17	1.17	1.16	1.20	1.19	1.21
6080–6030	3.36	1.96	**0.92**	**0.95**	1.56	1.95	1.41	1.45
5100–4910	2.40	1.47	2.90	2.91	2.82	2.66	2.90	2.81

Table 2
IBU-NIC model: A matrix of RMSEP values of the PLS regression models when using different regions and different levels of chemometrics (Bold = top ten models).

Region (Wavenumber cm^{-1})	RMSEP Values (%)							
	Original	SNV	1st Dev. SNV	1st Dev. SNV SGS	1st Dev. SNV NS	2nd Dev. SNV	2nd Dev. SNV SGS	2nd Dev. SNV NS
10000–5400	11.80	0.91	1.52	1.52	**1.37**	1.88	1.73	1.64
10000–4000	4.61	1.74	3.13	3.12	2.29	3.57	3.38	2.69
9000–8000	12.50	1.84	**1.54**	**1.59**	1.48	**1.60**	**1.80**	1.93
9000–4700	3.57	1.10	1.78	1.78	**1.42**	1.93	**1.74**	1.70
7450–7000	9.82	4.34	1.28	1.26	1.77	1.57	1.52	**0.95**
6820–6620	4.64	2.99	2.18	2.17	2.50	4.72	2.69	2.47
6100–5600	4.58	1.96	1.67	1.68	1.44	1.88	1.80	1.56
6080–6030	3.03	1.52	**0.92**	**0.94**	1.20	1.69	1.62	1.48
5100–4910	2.86	1.60	3.23	3.23	3.33	2.86	2.92	3.00

Table 3
IBU-NIC model: The top ten PLS regression models in order of RMSEC value. The RMSEP and the difference between RMSEC and RMSEP are also shown along with the regions and chemometrics used.

Model	Region (cm^{-1})	Chemometrics	RMSEC (%)	RMSEP (%)	RMSEC – RMSEP (%)	Corr. Coef.
1	7450–7000	SNV, 2nd Dev., NS	0.77	0.95	−0.18	0.9997
2	9000–8000	SNV, 1st Dev.	0.87	1.54	−0.67	0.9996
3	9000–8000	SNV, 2nd Dev.	0.89	1.60	−0.71	0.9996
4	9000–8000	SNV, 1st Dev., SGS	0.90	1.59	−0.69	0.9996
5	9000–4700	SNV, 1st Dev., NS	0.92	1.42	−0.50	0.9995
6	6080–6030	SNV, 1st Dev.	0.92	0.92	+0.00	0.9995
7	6080–6030	SNV, 1st Dev., SGS	0.95	0.94	+0.01	0.9995
8	9000–8000	SNV, 2nd Dev., SGS	0.96	1.80	−0.84	0.9995
9	9000–4700	SNV, 2nd Dev., SGS	0.96	1.74	−0.78	0.9995
10	10000–5400	SNV, 1st Dev., NS	0.97	1.37	−0.40	0.9995

Table 4
CBZ-NIC model: A matrix of RMSEC values of the PLS regression models when using different regions and different levels of chemometrics (Bold = top ten models).

Region (Wavenumber cm^{-1})	RMSEC Values (%)							
	Original	SNV	1st Dev. SNV	1st Dev. SNV SGS	1st Dev. SNV NS	2nd Dev. SNV	2nd Dev. SNV SGS	2nd Dev. SNV NS
10000–9646	5.01	3.16	**1.55**	**1.54**	2.37	**1.51**	**1.63**	2.67
10000–5400	6.99	2.40	3.42	2.49	2.49	**2.23**	3.29	2.46
10000–4000	6.46	2.76	2.84	2.84	2.77	2.86	2.94	2.80
9000–8500	7.10	3.28	**2.28**	**2.30**	2.42	**1.18**	**1.23**	**2.32**
9000–5300	6.88	2.60	2.52	2.52	2.51	2.44	2.55	2.49
7200–5400	6.35	2.68	2.58	2.58	2.58	2.59	2.62	2.56
6881–6696	5.26	3.18	2.68	2.68	2.66	2.70	2.68	2.57
6684–6457	5.58	2.52	2.58	2.58	2.58	2.56	2.59	2.60
6075–5827	6.25	3.21	3.26	3.26	3.33	2.82	2.95	3.31

mation and 99.7% concentration information. The second factor used 0.5% spectral and 0.2% concentration information.

The 2nd Dev. NIR spectral region, 7450–7000 cm^{-1}, used for Model 1 is shown in Fig. 7. This region exhibited clear and predictable differences between each spectrum. The majority of the observed bands in this range showed an increase in absorbance intensity as the 1:1 IBU-NIC CC concentration was decreased from 100% co-crystal to 0% (pure ibuprofen).

It was difficult to identify individual bands within the NIR spectra because most are overtone or combination bands. The hydrogen bonding involved in forming the IBU-NIC CC may have caused some of the observed band shifting. The most significant shift in the shown region was from 7108 cm^{-1} to 7128 cm^{-1}. Two other shifts were seen from 7070 cm^{-1} to 7081 cm^{-1} and from 7378 cm^{-1} to 7367 cm^{-1}.

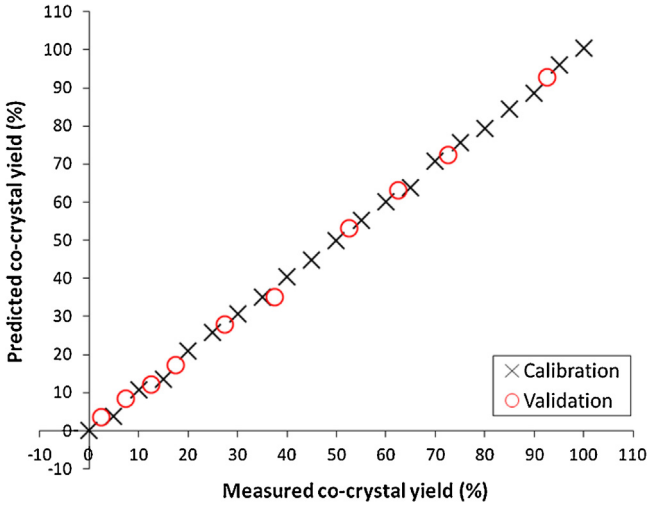

Fig. 6. IBU-NIC model: PLS regression Model 1. Using the region 7450–7000 cm^{-1} and chemometrics 2nd Dev., SNV and Norris Smoothing.

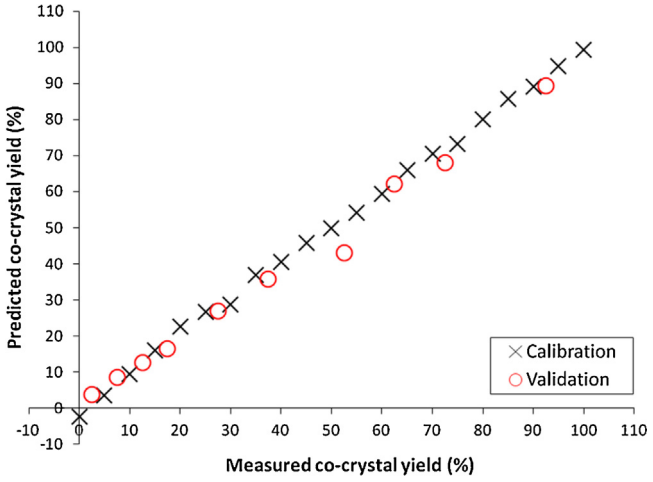

Fig. 8. CBZ-NIC model: PLS regression Model 2. Using the region 9000–8500 cm^{-1} and chemometrics 2nd Dev., SNV and SG Smoothing.

5. CBZ-NIC PLS model

The RMSEC, RMSEP and correlation coefficient values were recorded for each region and various degrees of chemometric pre-treatments were used. Tables 4 and 5 display the RMSEC and RMSEP values for each regression model respectively. The chemometric pre-treatments that were applied had a similar effect to the IBU-NIC model, with the SNV being important for reducing both error values. Again, the different evaluated regions reacted differently to the various levels of chemometrics. The ten models with the lowest RMSEC values are highlighted in bold to help visualise their distribution related to the different chemometrics that were applied.

Table 6 shows the ten PLS regression models which exhibited the lowest RMSEC values. According to the correlation coefficient values, the models were well correlated linear models.

The wavenumber region of 9000–8500 cm^{-1} provided the first and second smallest calibration errors of 1.18% (Model 1) and 1.23% (Model 2). This region provided a model with relatively low error values which could accurately predict the percentage yield of 1:1 CBZ-NIC CC in samples where there is a mixture of carbamazepine and the 1:1 CC.

The best overall performing model was determined as Model 2. Model 2 was chosen because it exhibited a small RMSEP value of 3.53% compared to 4.26% for Model 1. The difference between the RMSEC and RMSEP value was only −2.30% for Model 2 where as it was significantly larger for Model 1, −3.08%. Model 2 is plotted in Fig. 8. Both the averaged calibration and validation samples are shown to compare the measured co-crystal yield to the PLS regression predicted co-crystal yield. This model had a correlation coefficient of 0.9992. An outlying point was observed for the validation sample 52.5% CBZ-NIC CC yield.

The spectral and concentration factor loadings for both PLS factors were calculated. The first factor used 95.1% spectral information and 99.4% concentration information. The second factor used 0.6% spectral and 0.4% concentration information.

The 2nd Dev. NIR spectral region, 9000–8500 cm^{-1}, used for Model 2 is shown in Fig. 9. The majority of the observed bands in this region exhibited an increase in absorbance intensity as the 1:1 CBZ-NIC CC concentration was decreased from 100% to 0% (pure carbamazepine). It may be possible that the hydrogen bonding involved in forming the 1:1 CBZ-NIC CC may have caused some of the observed band shifting. The band shifting for this system is more subtle compared to the ibuprofen-nicotinamide system. The most significant observed shift is from 8690 cm^{-1} to 8705 cm^{-1}.

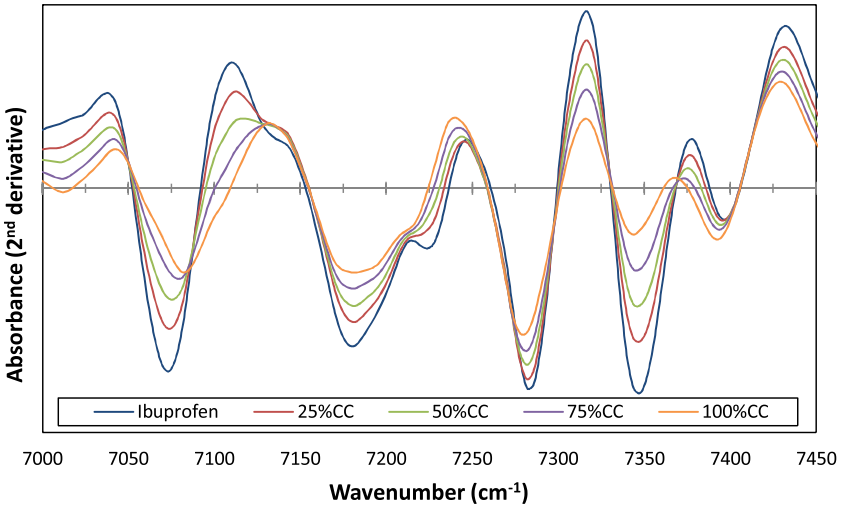

Fig. 7. IBU-NIC model: 2nd derivative NIR spectra over the region 7450–7000 cm^{-1} with Norris smoothing of ibuprofen and the calibration samples with 25, 50, 75 and 100% 1:1 IBU-NIC CC.

Table 5
CBZ-NIC model: A matrix of RMSEP values of the PLS regression models when using different regions and different levels of chemometrics (Bold= top ten models).

Region (Wavenumber cm^{-1})	RMSEP Values (%)							
	Original	SNV	1st Dev. SNV	1st Dev. SNV SGS	1st Dev. SNV NS	2nd Dev. SNV	2nd Dev. SNV SGS	2nd Dev. SNV NS
10000–9646	3.29	3.59	**3.92**	**4.00**	3.04	**5.49**	**4.73**	3.71
10000–5400	5.03	2.71	4.22	3.09	3.11	**3.07**	4.52	3.00
10000–4000	5.59	3.51	4.20	4.21	3.91	4.58	4.51	4.09
9000–8500	4.26	4.28	**3.32**	**3.32**	3.30	**4.26**	**3.53**	**3.33**
9000–5300	4.97	3.00	3.13	3.13	3.15	3.04	3.08	3.03
7200–5400	4.87	3.12	3.18	3.18	3.20	3.09	3.13	3.10
6881–6696	4.44	3.95	3.41	3.41	3.36	3.41	3.33	3.11
6684–6457	4.08	2.99	3.00	3.00	2.98	3.15	3.07	2.99
6075–5827	5.05	4.23	4.12	4.12	4.34	3.42	3.69	4.34

Table 6
CBZ-NIC model: The top ten PLS regression models in order of RMSEC value. The RMSEP and the difference between RMSEC and RMSEP are also shown along with the regions and chemometrics used.

Model	Region (cm^{-1})	Chemometrics	RMSEC (%)	RMSEP (%)	RMSEC – RMSEP (%)	Corr. Coef.
1	9000–8500	SNV, 2nd Dev.	1.18	4.26	−3.08	0.9992
2	9000–8500	SNV, 2nd Dev., SGS	1.23	3.53	−2.30	0.9992
3	10000–9646	SNV, 2nd Dev.	1.51	5.49	−3.98	0.9988
4	10000–9646	SNV, 1st Dev., SGS	1.54	4.00	−2.46	0.9987
5	10000–9646	SNV, 1st Dev.	1.55	3.92	−2.37	0.9987
6	10000–9646	SNV, 2nd Dev., SGS	1.63	4.73	−3.10	0.9985
7	10000–5400	SNV, 2nd Dev.	2.23	3.07	−0.84	0.9973
8	9000–8500	SNV, 1st Dev.	2.28	3.32	−1.04	0.9972
9	9000–8500	SNV, 1st Dev., SGS	2.30	3.32	−1.02	0.9971
10	9000–8500	SNV, 2nd Dev., NS	2.32	3.33	−1.01	0.9971

Table 7
A comparison of the selected 1:1 IBU-NIC model (Model 1) and 1:1 CBZ-NIC model (Model 2), including the region, number of factors, chemometrics, RMSEC, RMSEP and correlation coefficient.

Co-crystal Pair	Region (cm^{-1})	PLS Factors	Chemometrics	RMSEC (%)	RMSEP (%)	Corr. Coef.
1:1 IBU-NIC	7450–7000	2	SNV, 2nd Dev., NS	0.77	0.95	0.9997
1:1 CBZ-NIC	9000–8500	2	SNV, 2nd Dev., SGS	1.23	3.53	0.9992

The most prominent band associated with the co-crystal in this region was situated at 8751 cm^{-1}.

6. Model comparison

To compare both co-crystal pairs, the selected model details are shown in Table 7. The correlation coefficient, RMSEC and RMSEP values were compared. Both co-crystal pairs achieved linear models with relatively low error values. In summary, the 1:1 IBU-NIC model had lower RMSEC and RMSEP values than the 1:1 CBZ-NIC model.

For the 1:1 CBZ-NIC model, the validation sample data point with a 52.5% measured co-crystal yield in Fig. 8 could be an outlier as it deviates from the linear model significantly more than any other data point. The squared residual for this point was 2.4 times larger than the sum of the squared residuals for the validation set when excluding the outlier. If this data point is removed

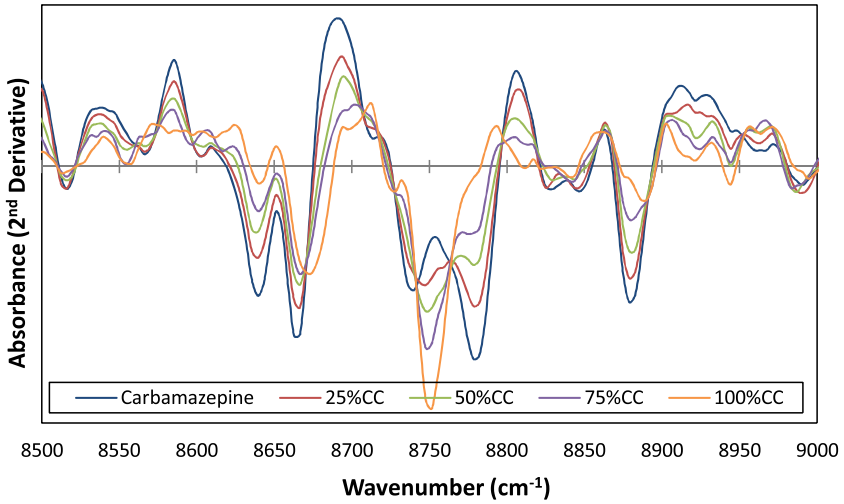

Fig. 9. CBZ-NIC model: 2nd derivative NIR spectra over the region 9000–8500 cm^{-1} with SG smoothing of carbamazepine and the calibration samples with 25, 50, 75 and 100% 1:1 CBZ-NIC co-crystal.

from the validation set, the RMSEP value improves from 3.53% to 2.02% when using all of the same conditions: SNV, 2nd Dev., SGS, region 9000–8500 cm^{-1}. This would bring the 1:1 CBZ-NIC model closer to the 1:1 IBU-NIC model when comparing prediction error.

Regarding the 2nd Dev. NIR spectra shown in Figs. 7 and 9, the majority of bands exhibited an increase in intensity as the co-crystal concentration decreased over the observed ranges. It is important to note that over different spectral ranges not used for the chosen models, there were NIR bands with increased intensity due to an increase in the co-crystal concentration. This could suggest the PLS models have reduced error values over a region where the intensity of most NIR bands directly correlates to a decrease in the co-crystal concentration.

The 2nd Dev. 1:1 CBZ-NIC spectra used to create the models were relatively complex and exhibited more subtle differences between each co-crystal concentration, compared to the 1:1 IBU-NIC spectra. The complex 1:1 CBZ-NIC spectra could be caused by the different arrangement of hydrogen bonding associated with the co-crystal compared to the 1:1 IBU-NIC CC. This complexity could have impacted the PLS regression and may have been the reason why the error values were higher for the selected 1:1 CBZ-NIC model.

7. Conclusion

The results demonstrate that NIR spectroscopy can be used to accurately distinguish between the individual components and the co-crystal form of two different pharmaceutical co-crystal pairs. Clear differences in the NIR spectra were observed when shown in the second derivative, and varying levels of chemometrics enabled the PLS regression to achieve relatively low calibration and validation error values. The findings suggest that NIR spectroscopy could be utilised as an accurate PAT tool for pharmaceutical co-crystal manufacturing methods and could aid understanding of the cocrystallization process.

Acknowledgements

This work was funded by the Engineering and Physical Sciences Research Council, UK; grant code EP/J003360/1.

Appendix A.

$$\mathrm{RMSEC} = \sqrt{\sum_{i=1}^{N_C} \frac{\left(\hat{Y}_{Ci} - Y_i\right)^2}{N_C}} \quad (1)$$

Eq. (1) shows the relationship between the root mean square error of calibration and the predictions of the calibration samples $\hat{Y}_{Ci}$ the measured concentration of the sample Y_i and the number of samples in the calibration set N_C

$$\mathrm{RMSEP} = \sqrt{\sum_{i=1}^{N_P} \frac{\left(\hat{Y}_{Pi} - Y_i\right)^2}{N_V}} \quad (2)$$

Eq. (2) shows the relationship between the root mean square error of prediction and the predictions of the validation samples $\hat{Y}_{Pi}$, the measured concentration of the sample Y_i and the number of samples in the validation set N_V.

Appendix B. Supplementary data

Supplementary data associated with this article can be found, in the online version, at http://dx.doi.org/10.1016/j.jpba.2016.06.010.

References

[1] D. Food, Administration, Guidance for Industry PAT—a Framework for Innovative Pharmaceutical Development, Manufacturing, and Quality Assurance, DHHS, Rockville, MD, 2004.
[2] T. De Beer, A. Burggraeve, M. Fonteyne, L. Saerens, J.P. Remon, C. Vervaet, Near infrared and Raman spectroscopy for the in-process monitoring of pharmaceutical production processes, Int. J. Pharm. 417 (2011) 32–47.
[3] A. Rathore, R. Bhambure, V. Ghare, Process analytical technology (PAT) for biopharmaceutical products, Anal. Bioanal. Chem. 398 (2010) 137–154.
[4] K.A. Bakeev, Process Analytical Technology: Spectroscopic Tools and Implementation Strategies for the Chemical and Pharmaceutical Industries, John Wiley & Sons, 2010.
[5] M. Blanco, J. Coello, H. Iturriaga, S. Maspoch, C. de la Pezuela, Near-infrared spectroscopy in the pharmaceutical industry, Crit. Rev. Anal. 123 (1998) 135R–150R.
[6] F.H. Long, Vibrational Spectroscopic Methods for Quantitative Analysis, Handbook of Stability Testing in Pharmaceutical Development, Springer, 2009, pp. 223–240.
[7] G. Reich, Near-infrared spectroscopy and imaging: basic principles and pharmaceutical applications, Adv. Drug Deliv. Rev. 57 (2005) 1109–1143.
[8] R.A. Storey, I. Ymen, Solid State Characterization of Pharmaceuticals, Wiley Online Library, 2011.
[9] R. Caliandro, G. Di Profio, O. Nicolotti, Multivariate analysis of quaternary carbamazepine–saccharin mixtures by X-ray diffraction and infrared spectroscopy, J. Pharm. Biomed. Anal. 78 (2013) 269–279.
[10] F.L.F. Soares, R.L. Carneiro, Evaluation of analytical tools and multivariate methods for quantification of co-former crystals in ibuprofen-nicotinamide co-crystals, J. Pharm. Biomed. Anal. 89 (2014) 166–175.
[11] K. Faber, B.R. Kowalski, Propagation of measurement errors for the validation of predictions obtained by principal component regression and partial least squares, J. Chemom. 11 (1997) 181–238.
[12] N. Qiao, M. Li, W. Schlindwein, N. Malek, A. Davies, G. Trappitt, Pharmaceutical cocrystals: an overview, Int. J. Pharm. 419 (2011) 1–11.
[13] S. Aitipamula, R. Banerjee, A.K. Bansal, K. Biradha, M.L. Cheney, A.R. Choudhury, G.R. Desiraju, A.G. Dikundwar, R. Dubey, N. Duggirala, Polymorphs, salts, and cocrystals: what's in a name? Cryst. Growth Des. 12 (2012) 2147–2152.
[14] N. Blagden, M. De Matas, P. Gavan, P. York, Crystal engineering of active pharmaceutical ingredients to improve solubility and dissolution rates, Adv. Drug Deliv. Rev. 59 (2007) 617–630.
[15] C.B. Aakery, D.J. Salmon, Building co-crystals with molecular sense and supramolecular sensibility, CrystEngComm 7 (2005) 439–448.
[16] G.G. Zhang, R.F. Henry, T.B. Borchardt, X. Lou, Efficient co-crystal screening using solution-mediated phase transformation, J. Pharm. Sci. 96 (2007) 990–995.
[17] A.V. Trask, W. Jones, Crystal Engineering of Organic Cocrystals by the Solid-state Grinding Approach, Organic Solid State Reactions, Springer, 2005, pp. 41–70.
[18] T. Friščić, L. Fábián, J.C. Burley, W. Jones, W.S. Motherwell, Exploring cocrystal–cocrystal reactivity via liquid-assisted grinding: the assembling of racemic and dismantling of enantiomeric cocrystals, Chem. Commun. 48 (2006) 5009–5011.
[19] A.V. Trask, W.S. Motherwell, W. Jones, Solvent-drop grinding: green polymorph control of cocrystallisation, Chem. Commun. (2004) 890–891.
[20] R.S. Dhumal, A.L. Kelly, P. York, P.D. Coates, A. Paradkar, Cocrystalization and simultaneous agglomeration using hot melt extrusion, Pharm. Res. 27 (2010) 2725–2733.
[21] S. Aher, R. Dhumal, K. Mahadik, A. Paradkar, P. York, Ultrasound assisted cocrystallization from solution (USSC) containing a non-congruently soluble cocrystal component pair: caffeine/maleic acid, Eur. J. Pharm. Sci. 41 (2010) 597–602.
[22] A.L. Kelly, T. Gough, R. Dhumal, S. Halsey, A. Paradkar, Monitoring ibuprofen–nicotinamide cocrystal formation during solvent free continuous cocrystallization (SFCC) using near infrared spectroscopy as a PAT tool, Int. J. Pharm. 426 (2012) 15–20.
[23] H.G. Moradiya, M.T. Islam, S. Halsey, M. Maniruzzaman, B.Z. Chowdhry, M.J. Snowden, D. Douroumis, Continuous cocrystallisation of carbamazepine and trans-cinnamic acid via melt extrusion processing, CrystEngComm 16 (2014) 3573–3583.
[24] M.C. Sarraguça, P.R. Ribeiro, A.O. Santos, M.C. Silva, J.A. Lopes, A PAT approach for the on-line monitoring of pharmaceutical co-crystals formation with near infrared spectroscopy, Int. J. Pharm. 471 (2014) 478–484.
[25] M.C. Sarraguça, P.R. Ribeiro, A.O.D. Santos, J.A. Lopes, Batch statistical process monitoring approach to a cocrystallization process, J. Pharm. Sci. 104 (2015) 4099–4108.
[26] M.C. Sarraguça, M. Paisana, J. Pinto, J.A. Lopes, Real-time monitoring of cocrystallization processes by solvent evaporation: a near infrared study, Eur. J. Pharm. Sci. 90 (2015) 76–84.
[27] M.-J. Lee, I.-C. Wang, M.-J. Kim, P. Kim, K.-H. Song, N.-H. Chun, H.-G. Park, G.J. Choi, Controlling the polymorphism of carbamazepine-saccharin cocrystals formed during antisolvent cocrystallization using kinetic parameters, Korean J. Chem. Eng. 32 (2015) 1910–1917.

[28] N.-H. Chun, M.-J. Lee, G.-H. Song, K.-Y. Chang, C.-S. Kim, G.J. Choi, Combined anti-solvent and cooling method of manufacturing indomethacin–saccharin (IMC–SAC) co-crystal powders, J. Cryst. Growth 408 (2014) 112–118.
[29] K. Tripathi, Essentials of Medical Pharmacology, J.P. Medical Ltd., 2013.
[30] M. Yazdanian, K. Briggs, C. Jankovsky, A. Hawi, The high solubility definition of the current FDA guidance on biopharmaceutical classification system may be too strict for acidic drugs, Pharm. Res. 21 (2004) 293–299.
[31] N.A. Kasim, M. Whitehouse, C. Ramachandran, M. Bermejo, H. Lennernäs, A.S. Hussain, H.E. Junginger, S.A. Stavchansky, K.K. Midha, V.P. Shah, Molecular properties of WHO essential drugs and provisional biopharmaceutical classification, Mol. Pharm. 1 (2004) 85–96.
[32] D.J. Good, N.r. Rodriíguez-Hornedo, Solubility advantage of pharmaceutical cocrystals, Cryst. Growth Des. 9 (2009) 2252–2264.
[33] N. Blagden, D.J. Berry, A. Parkin, H. Javed, A. Ibrahim, P.T. Gavan, L.L. De Matos, C.C. Seaton, Current directions in co-crystal growth, New J. Chem. 32 (2008) 1659–1672.
[34] S.G. Fleischman, S.S. Kuduva, J.A. McMahon, B. Moulton, R.D. Bailey Walsh, N. Rodríguez-Hornedo, M.J. Zaworotko, Crystal engineering of the composition of pharmaceutical phases: multiple-component crystalline solids involving carbamazepine, Cryst. Growth Des. 3 (2003) 909–919.
[35] F. Allen, The Cambridge structural database: a quarter of a million crystal structures and rising, Acta Crystallogr. Sec. B 58 (2002) 380–388.
[36] D.J. Berry, C.C. Seaton, W. Clegg, R.W. Harrington, S.J. Coles, P.N. Horton, M.B. Hursthouse, R. Storey, W. Jones, T. Friscic, Applying hot-stage microscopy to co-crystal screening: a study of nicotinamide with seven active pharmaceutical ingredients, Cryst. Growth Des. 8 (2008) 1697–1712.
[37] A. Shayanfar, S. Velaga, A. Jouyban, Solubility of carbamazepine, nicotinamide and carbamazepine–nicotinamide cocrystal in ethanol–water mixtures, Fluid Phase Equilib. 363 (2014) 97–105.
[38] R. Barnes, M. Dhanoa, S.J. Lister, Standard normal variate transformation and de-trending of near-infrared diffuse reflectance spectra, Appl. Spectrosc. 43 (1989) 772–777.
[39] A. Savitzky, M.J. Golay, Smoothing and differentiation of data by simplified least squares procedures, Anal. Chem. 36 (1964) 1627–1639.
[40] K. Norris, P. Williams, Optimization of mathematical treatments of raw near-infrared signal in the measurement of protein in hard red spring wheat. I Influence of particle size, Cereal Chem. 61 (1984) 158–165.